

# A Simulation Platform for Small Solar System Bodies using the Einstein-Elevator

E. Tahtali,<sup>1</sup> C. Kreuzig,<sup>2</sup> G. Meier,<sup>2</sup> J. Blum,<sup>2</sup> L. Overmeyer,<sup>1</sup> and C. Lotz<sup>1</sup>

<sup>1</sup>*Leibniz University Hannover, Institute of Transport and Automation Technology, An der Universitaet 2, 30823 Garbsen, Germany*

<sup>2</sup>*Technische Universität Braunschweig, Institute of Geophysics and Extraterrestrial Physics, Mendelssohnstr. 3, 38106 Braunschweig, Germany*

(\*Electronic mail: emre.tahtali@ita.uni-hannover.de)

(Dated: 17 November 2025)

Small solar system bodies are becoming increasingly important as missions like NASA's OSIRIS-REx show. However, the study of the characteristics and behavior of these objects on Earth is a challenge as the simulation of their environmental condition is difficult. We present in this paper an approach to enable the simulation of SSSB conditions in a drop tower facility on Earth, which is being addressed as part of the AKUS ("Activity of Comets under Partial Gravity") project. This especially concerns their prevailing gravity levels, which range between  $10^{-2} g$  and  $10^{-4} g$ . In order to simulate the conditions of SSSB as accurately as possible, an acceleration system based on servo motors and spindle axes has been developed. The accelerations will be transferred from the motors to the spindle axes containing a comet-like sample. These are together placed inside a vacuum chamber providing a vacuum quality of  $10^{-6}$  mbar. The whole setup will be installed inside the Einstein-Elevator. Our results show that, with the current setup, we are able to generate conditions from  $10^{-2} g$  down to  $10^{-3} g$ . The maximum deviations under these conditions are  $\pm 5 \cdot 10^{-4} g$ . Additionally, this setup is offering the opportunity to conduct different kinds of experiments in which the described gravity levels and vacuum conditions are needed.

## I. INTRODUCTION

Space research has always played an important role for humankind. Beginning with the understanding of the night sky and the movement of stars and planets in the antiquity, the interest increased with the space age. In this context, small solar system bodies (SSSB), for instance comets or asteroids, also became a growing field of interest. These objects play a major role in the understanding of the solar system's formation as ancient celestial bodies. Moreover, they are relevant as future resources and a potential impact threat to Earth. Their importance is underscored by NASA missions such as "Double Asteroid Redirection Test" (DART) or "Origins, Spectral Interpretation, Resource Identification, Security, Regolith Explorer" (OSIRIS-REx)<sup>1-4</sup>. Although these kinds of missions and the gained data are very important and valuable, they also have major disadvantages. Firstly, the mentioned missions are expensive and planning-intensive. The costs can amount to several billion dollars with a planning time of a decade or more. Despite the cost and the planning, they have a high residual risk of failing. As a result, alternative options have to be developed to make comet research more accessible. While there are some comet research facilities which simulate the temperature and vacuum conditions of SSSB, an environment of ambient  $g$ -levels between  $10^{-2}$  to  $10^{-4}$  is seldom given due to Earth's overwhelming gravity<sup>5-7</sup>. However, the most similar  $g$ -level is the provision of microgravity. In this context, there are several alternative options, for instance parabolic flights, sounding rockets or drop towers<sup>8,9</sup>. The most promising of these are drop towers considering their microgravity quality, availability, repeatability and the flight cost. For the implementation of an additional artificial force and therefore a simulated gravity, a centrifuge or propulsion system can be used during the microgravity time of the drop tower. The

Einstein-Elevator (EE), as a third generation drop tower, offers the possibility to implement an additional propulsion system, especially due to its high repeatability rate of 100 flights per day and its microgravity quality of  $10^{-6} g$ <sup>10</sup>. With this implementation, an alternative opportunity is given to conduct SSSB simulations and particularly comet-relevant experiments. In connection with this, the here presented paper gives an overview regarding the state of the art of SSSB simulation platforms/laboratories (Sect. II), followed by a detailed description of the experiment AKUS ("Activity of Comets under Partial Gravity") and its experimental environment (Sect. III). Subsequently, first test results are presented, which serve as proof of concept (Sect. IV). Ultimately, the discussion provides a scientific evaluation of the results (Sect. V), ending with a conclusion and outlook on the potential of the presented system (Sect. VI) and its use for a better understanding of SSSB.

## II. SCIENTIFIC BACKGROUND AND MOTIVATION

SSSB research relies mostly on observations from Earth or on space missions such as Rosetta or OSIRIS-REx<sup>11-14</sup>. Considering the investigation of comets for instance, the data collected by Rosetta are of high value. Nevertheless, there are many aspects that still have to be examined. In particular, regarding comet surface activity, several influences still have to be quantified to fully understand the ejection process of the volatiles/particles. These include, for instance, the temperature associated with solar radiation or its own gravity. In this context, there are several simulation facilities and laboratories that can be used for SSSB research since they allow the simulation of the gravity levels, the vacuum, the temperature or a combination out of these. In general, these can be divided

into those that are subject to Earth's gravity and those where gravity can be adjusted. In the following, three examples of SSSB laboratories/platforms will be highlighted. These examples focus on different relevant environmental conditions and are connected to the work presented in this paper. One of them is the Comet Physics Laboratory (CoPhyLab) at the Technische Universität Braunschweig, which functions as a basis concept of our work together with the experiments related to it (in Sect. II A). As a result, AKUS enables sister experiments of those in the CoPhyLab. In addition, the cold gas propulsion system at Beijing Drop Tower, in which SSSB research is possible, (in Sect. II B) and the controlled partial gravity platform at ZARM, in which SSSB experiments have been conducted, (in Sect. II C) will be presented. These two stand out since they offer adjustable gravity levels relevant to SSSB research. However, those differ from each other as they have different acceleration concepts, sizes and experimental environments.

### A. CoPhyLab

The CoPhyLab is an international research project started in 2018. The main laboratory is located at the Technische Universität Braunschweig and the project partners are the IWF Graz and the Universität Bern. The aim of CoPhyLab is the understanding of the basic physics behind cometary activity. Therefore, laboratory experiments with simple sample compositions are performed and supplemented by thermophysical models. The heart of the laboratory is the CoPhyLab L-Chamber<sup>5</sup>. In this chamber samples can be kept at temperatures below 150 K and in high vacuum, providing the same conditions comets experience on their approach to the Sun. The Sun is simulated using a halogen lamp. In the L-Chamber a total of 14 instruments can be used to measure different properties of the sample and its evolution under illumination. In addition to the L-Chamber, several smaller chambers are available in the CoPhyLab-consortium, which provide the same conditions, but have only a few instruments attached. This reduces the operational complexity, allowing for parameter studies with many different kinds of samples and illumination patterns.<sup>15</sup>

The most common volatile material on comets is water ice, which is found in micrometer-sized particles mixed within the other volatiles and refractory materials<sup>16</sup>. Such ice particles are produced in the CoPhyLab using a custom-made ice machine<sup>17</sup>. These water-ice particles eject particles of themselves under illumination in high vacuum, which is an effect studied in all CoPhyLab chambers<sup>15</sup>. This ejection process is not fully understood until now. However, one parameter, which has not been investigated yet, is gravity. This is important because the particles must overcome their own weight and tensile strength before they can be released. On a comet, the gravity is several orders of magnitude lower. Hence, much bigger particles can be ejected. The largest observed ejected particles in the CoPhyLab are a few hundred micrometers in size, but by reducing gravity, these particles could be larger,

unless their size is defined by other processes. Further, the ejection of dust particles is finite in the laboratory, but comets eject dust particles continuously if they are close to the Sun. This can be caused by gravity on Earth, because the dust particles are denser and therefore heavier than ice particles. If this is true, experiments with reduced gravity should remain active but if their activity also stops, the sample composition or structure must be different to that of a comet, necessitating further research into those parameters.

### B. Cold gas propulsion system at Beijing Drop Tower

The necessity of adjustable gravity ranges for SSSB research have been indicated in Sect. II A especially regarding their surface activity. A propulsion system that is capable of generating gravity levels from  $10^{-3}$  to  $10^{-5}$  g has been developed at Beijing Drop Tower, consisting of an inner and outer capsule (two-capsule system)<sup>9,18,19</sup>. During the 3.6 s long drop of the capsule, cold-gas thrusters are activated, which are attached at the bottom of the inner capsule of the system. The thrusters, which use de Laval nozzles, vary in their geometries to generate the desired accelerations. In total, 24 thrusters have been installed with different amounts of thrust, specifically four 50 mN and 20 100 mN thrusters, so that the applicable thrust ranges between 200 mN and 2.000 mN. To achieve  $10^{-4}$  g, the group of 50 mN thrusters are activated, whereby all 100 mN thrusters are used to achieve a gravity level of  $10^{-3}$  g. However, results of a test flight, in which all thrusters have been activated, have not been published yet. Moreover, due to the design of the nozzle layout, it is difficult to adjust different g-levels by activating the nozzles separately. This is because of a rotational force that could act on the experimental platform and could harm the infrastructure. The generated acceleration is measured using an acceleration sensor, which is placed inside the inner capsule. Although the platform, as described, can enable gravity levels of SSSB, research or experiments in this area have also not been published yet.

### C. Controlled partial gravity platform at ZARM

Another platform, in which SSSB-relevant experiments have already been conducted, has been developed for the GraviTower (GTB) and ZARM drop tower in Bremen, namely the "Controlled Partial Gravity Platform for Milligravity"<sup>20-22</sup>. The platform is built for asteroid impact investigations and consists of several components such as the actuation components, a vacuum chamber with the needed pumping stages, a launcher which pushes the impactor on the granular bed and cameras together with a lighting system that observe the impact. Its acceleration system consists of one linear motor translation stage, which is typically used for applications in the field of optics. The travel distance of the system is 300 mm, enabling different experiment times depending on the used drop tower<sup>20</sup>. The limits resulting from its length are primarily found in the higher acceleration ranges.

If, for instance, an acceleration of  $10^{-2} g$  is desired, the experiment time is  $< 2$  s. At the GTB, due to its microgravity duration, the limits are at 2.5 s regardless of the adjusted gravity level. Nevertheless, with the use of the ZARM drop tower, the experiment time, depending on the chosen acceleration, can be up to 9.3 s. During the microgravity time, the linear stage accelerates the vacuum chamber together with the launcher and the acceleration is controlled via the encoder of the motors. The travel trajectory looks promising, as the travel residuals are small. However, additional sensor data, such as accelerometer data have not been published yet, even though they directly indicate the prevailing acceleration in the experiment area. This applies also for accelerations based on the encoder data.

### III. EXPERIMENTAL PLATFORM AND SETUP

For the conduction of the experiments within AKUS, a microgravity environment is necessary. The platform which provides this condition is the EE, a third generation drop tower. Therefore, the EE as the experimental environment of AKUS will be described first before the actual experimental setup of AKUS.

#### A. The Einstein-Elevator

The EE is a novel drop tower, which is used for quantum sensing, space and space-production related research<sup>23–26</sup>. It is located at Leibniz University Hannover. Due to its unique design, a microgravity quality of  $10^{-6} g$  as well as other gravity levels such as those on the Mars or Moon surface are achievable<sup>10</sup>. The facility is able to perform 300 flights per day (100 flights per 8 h-shift operation) as the gondola is the only volume which is evacuated to achieve vacuum and, as a result, an acoustic decoupling. Additionally, the EE is able to accelerate a payload with a total mass up to 1,000 kg and has a high degree of automation. Furthermore, it is able to contain experiments with a height of 2 m and a diameter of 1.7 m. Those key aspects are enabled by three main components that play a crucial role: the drives, the guidance system and the gondola that includes the experiment carrier within a vacuum atmosphere presented in FIG. 1. For the simulation of microgravity, the flight begins with a 5 g acceleration phase of 0.5 s, which is provided by the drives. A short deceleration phase follows to create a distance between the carrier and the gondola. This is the starting point for the microgravity period of 4 s. With the end of the microgravity time, the distance between the carrier and the gondola is reduced to zero again, so that the carrier and the gondola are reconnected. Afterwards, the gondola is decelerated with 5 g for 0.5 s, so that the gondola is arriving at its launching position<sup>8</sup>. Finally, the experiment carrier is centered again due to displacements caused by the Coriolis forces during the free-fall time and ending the flight. For our experiment, a high microgravity quality is necessary, as this is fundamental to add an artificial force, which simulates the gravity conditions of SSSB. The EE provides a

high microgravity quality, as the gondola and the drive guidance are separated due to the tower-in-tower design. With this, the transmission of vibrations into the experiment carrier, mainly caused by the drives, is reduced. The two components are only connected by a coupling rod. In addition, the foundation of both towers are separated from each other. The experiment carrier, designed as a pressure vessel, is important because it enables vacuum outside itself and thus inside the gondola<sup>27</sup>. As a consequence, experiments are at atmospheric pressure inside the carrier with an acoustic decoupling given by the vacuum outside of it, reducing the transmission of vibrations. In contrast to microgravity flights, the experiment carrier has to be attached to the gondola ground for gravity levels between  $\mu g$  to 1 g (hypogravity) and 1 g to 5 g (hypergravity). An adjustment of the trajectory of the gondola is required for the desired acceleration, directly influencing the duration of the test time. However, gravity levels of SSSB cannot be simulated by the EE's drives as those cannot regulate finely enough. Moreover, experiments can be conducted from the top starting position of the tower as an alternative option. Therefore, initial disturbances of the 5 g-acceleration phase can be avoided for acceleration-sensitive experiments, leading to a smoother and direct transition from 1 g to 0 g. Consequently, this also halves the microgravity time to 2 s.

#### B. Experimental setup of the AKUS experiment

Within this subsection, a general description of the AKUS-experiment will be given firstly. Afterwards, the acceleration system will be described in detail, as it is necessary to provide the gravity conditions of SSSB. Finally, the current graphical user interface (GUI) will be presented, since it will play a major role in the future regarding the monitoring of the system.

##### 1. General description of the Experiment

As previously described, the scientific goals of AKUS build on the experiments conducted inside the L-Chamber, but additionally utilizing the microgravity environment of the EE. As a result, gravity as a further important parameter and its influence can be examined with regard to the particle ejection of comets. This is in contrast to former experiments conducted under potentially masking Earth gravity conditions. To simulate the environmental conditions of comet surfaces in the EE, four main aspects of the experimental setup have to be highlighted, namely the mechanical components, the actuators, the sensors and the information processing. The first aspect consists of the vacuum chamber, which is used to achieve vacuum conditions up to  $10^{-6}$  mbar and is installed on the experiment carrier of the EE, seen in FIG. 2. Moreover, it contains several mechanical (e.g. for the actuators or the vacuum pump) or electrical interfaces (connection points for sensors and other electronic components). There are a total of two drive trains, each consisting of a motor, a rotary feedthrough and a spindle. Those two drive trains are connected to each other with a sample holder made of titanium, which was generatively de-

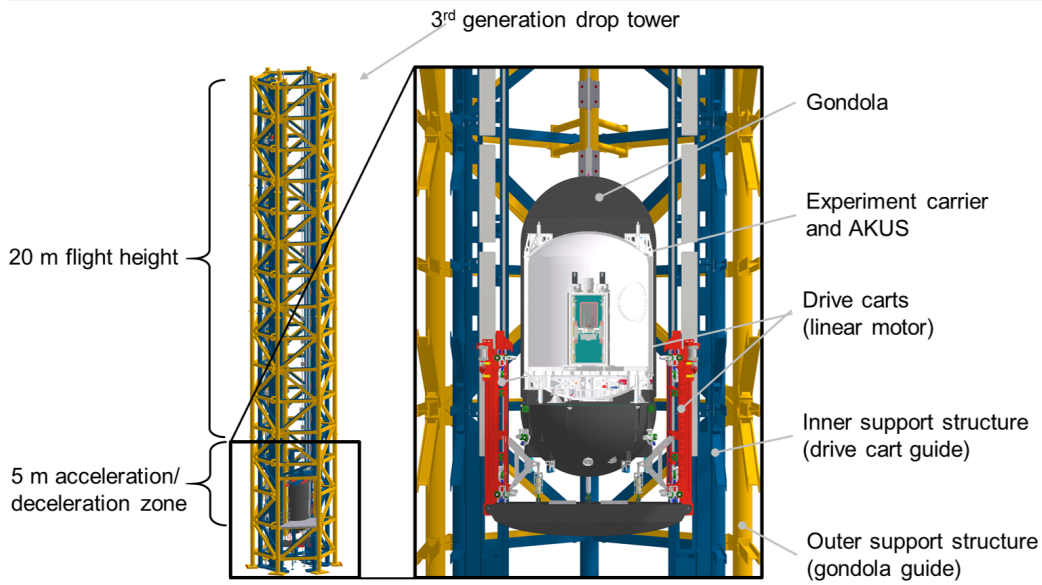
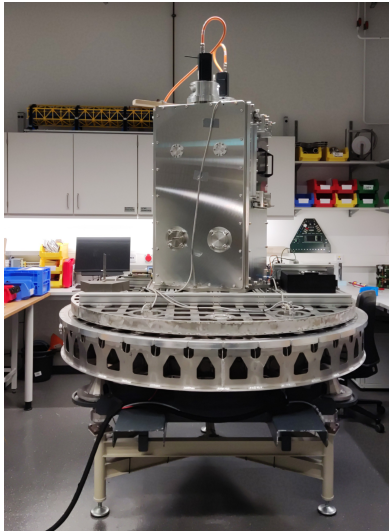
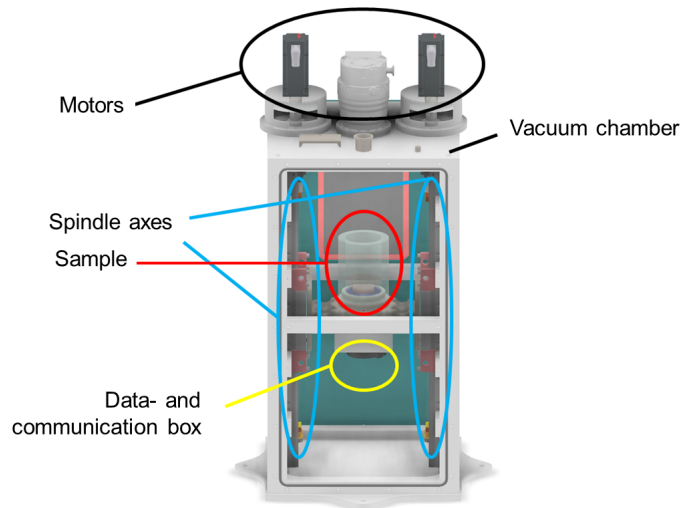


FIG. 1. The EE and its main components.



(a) The AKUS system build up on the bottom part of the experiment carrier.



(b) The main components used for AKUS.

FIG. 2. The AKUS system and its components.

signed for reasons of stability and low weight. The motors are placed outside of the vacuum chamber and connected via the feedthroughs to the vacuum-compatible spindles. During the free fall phase (approximately 0.5 s after the 5 g acceleration phase), the comet-like samples will be accelerated with the desired gravity level of SSSB, which is in the range of  $10^{-2}$  to  $10^{-4}$  g. While this acceleration is applied, the sample behavior will be observed by a cameras, which generate up to 75 fps. In addition to the cameras, other sensors are also installed such as temperature sensors, which are for instance connected to the sample, and an acceleration sensor, which is attached to the sample holder, seen in FIG. 3. Moreover, the

servo motors have encoders for the control of their dynamics. However, this will change in the long term, so that the controlled variable will be the acceleration signal supplied by the accelerometer which will be mounted close to the sample. For the data of the different sensors, a single-board computer (SBC) is installed inside a vacuum-compatible pressure chamber, the data- and communication box (FIG. 3 (b)). This pressure chamber is mounted directly under the sample holder and contains several other electrical components, for instance, AD or step-down converters. The data transfer from the SBC to the industrial PC (IPC), which controls the drives, are planed to be contactless. Possible data transfer methods still need to

be examined regarding its capabilities and transfer rate.

## 2. Detailed Design of the Acceleration System

The spindle axes used for our system have a travel distance of 680 mm. The choice of the length depended on two factors: firstly, the 4 s microgravity time of the EE, in which the whole process has to be conducted. Besides the constant acceleration, this includes the deceleration time of the carts. Secondly, the maximum travel distance resulting from the maximum acceleration of  $10^{-2} g$ , which is 600 mm at 3 s of acceleration time. Smaller accelerations are only limited by the microgravity time, as the travel length is long enough for several seconds of conducting time. In general, servo motors are not designed to achieve constant acceleration values, but rather to maintain a defined rotational speed or to achieve precise positioning. However, in our case, a stable acceleration torque is required to produce a constant linear acceleration. In the following, we will therefore briefly review the motion characteristics of servo motors and the relevant mechanical optimizations of our acceleration system.

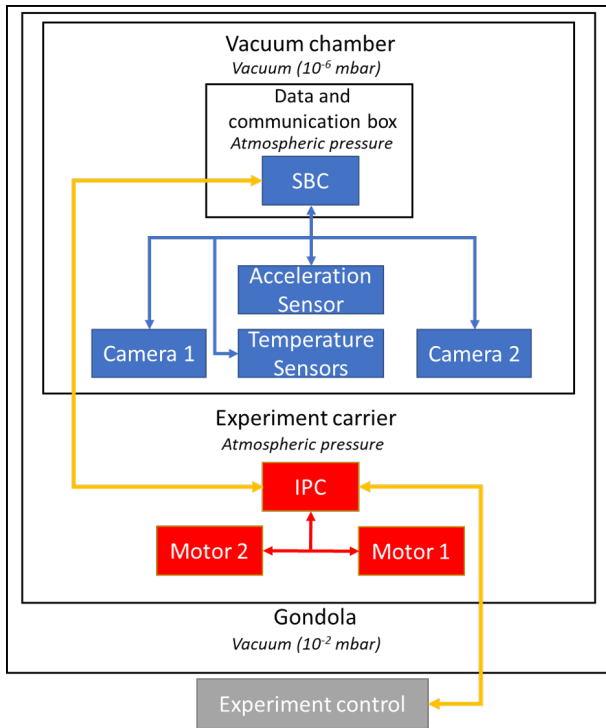


FIG. 3. General overview regarding the control components and their connections to each other

As described before, our servo motors are actuating the spindle axes and for the calculation of the desired torque, the following equation is the standard:

$$M_T = M_L + M_A. \quad (1)$$

Here  $M_T$  is the total torque, that the motor has to supply.  $M_L$  is the resulting torque caused by the load that is attached

on the drive train and therefore the spindle carts. Lastly,  $M_A$  is the acceleration torque and the most important in our case. The importance of the acceleration torque can be seen in the following equation:

$$M_A = J_T \cdot \alpha, \quad (2)$$

in which  $J_T$  is the total inertia and  $\alpha$  the angular acceleration of the motor. In addition,  $\alpha$  can be substituted as follows:

$$M_A = J_T \cdot \frac{\pi \cdot \Delta n}{30 \cdot \Delta t_A}. \quad (3)$$

$\Delta n$  is the difference of the rotational speed that should be achieved during the acceleration time  $\Delta t_A$ . As a consequence, it is the key factor that provides the desired acceleration of the sample. Considering our system without adjustments, the total inertia  $J_T$  of the load and the motors is approximately  $1.7 \cdot 10^{-4} \text{ kg}\cdot\text{m}^2$ . The rotational speed  $n$  accelerates from 0 to  $\approx 3600 \text{ /min}$  within a given time of 3 s. Based on these assumptions and using the Eq. (3), the acceleration torque results in  $\approx 0.0214 \text{ Nm}$ . With regard to our servo motor, the acceleration torque corresponds to  $\approx 1.65\%$  of the nominal torque (1.3 Nm). According to the manufacturer, the current controller can quantize to 1/1000 of the nominal torque. However, they suggest that for effective acceleration control, at least 100 increments are necessary (0.13 Nm). As a result, the current regulator of the motors cannot enable constant and small accelerations as the acceleration torque corresponds to  $\approx 16.5\%$  of the necessary torque (0.13 Nm). Hence, a constant acceleration is not possible as the motor inertia used in the former calculation is too small. This is also seen in FIG. 4. The motor accelerations are formed in high frequencies around the target value, whereby the amplitudes also increase, resulting in very noisy images. Additionally, servo motors and their controllers are primarily designed for position and velocity purposes. Torque control, especially in the lower regime, is not necessary, so the current resolution does not need to be very high.

One possibility to overcome this challenge is to increase the inertia of the system due to the framework conditions with respect to the microgravity time and the rotational speed based on the spindle axes. However, it should be emphasized that this approach also has some limitations in form of the inertia ratio  $\lambda$  of the motor  $J_M$  and the given load  $J_L$ <sup>28</sup> as seen in Eq. (4):

$$\lambda = \frac{J_L}{J_M}. \quad (4)$$

According to various motor developers, an inertia ratio of  $\lambda \leq 5$  should be aimed for a good motion behavior and control<sup>29,30</sup>. For this reason, the here used motors have adapted longer shafts, which already increases the motors' inertia. Due to the longer shafts, it is also possible to mount flywheels on the shafts with the aim of increasing the motor inertia and as a consequence the total inertia additionally.

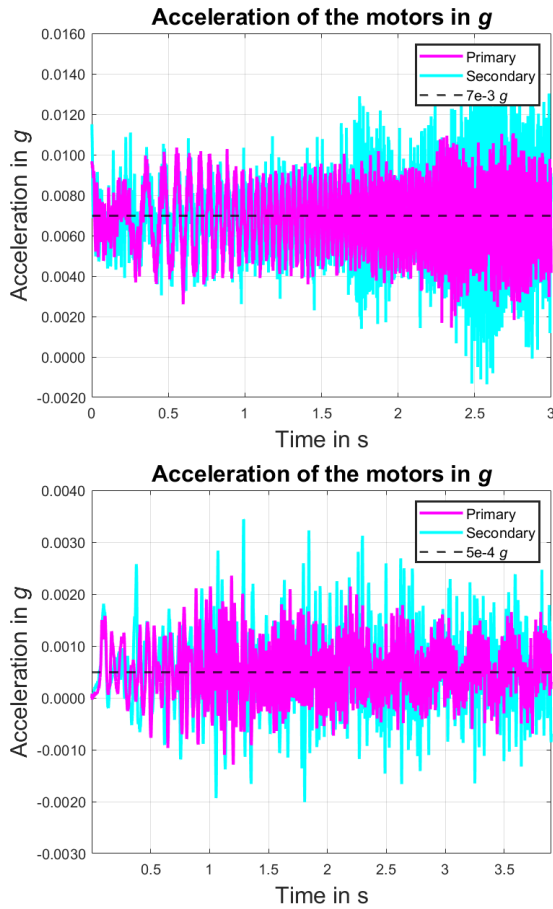


FIG. 4. Behavior of the motors regarding for  $7 \cdot 10^{-3} g$  (top) and  $5 \cdot 10^{-4} g$  (bottom)

These aluminum flywheels have a diameter of around 15 cm with a resulting inertia of  $J_F \approx 1.210 \cdot 10^{-3} \text{ kg m}^2$ . Based on Eq. (3), the resulting  $M_A$  is  $\approx 0.17 \text{ Nm}$ , so that at least 133 increments are given, which is, as stated before, necessary for a good control of the acceleration. The described mechanical adjustments have been used for the results presented in this manuscript in Sect. IV.

### 3. Graphical user interface (GUI)

To execute the experiment, a GUI has been developed. As the IPC and several automation components are products of the company Beckhoff, the GUI was built using TwinCat. The GUI contains several features to simplify the execution of the experiments, which are divided into three sections: experiment, manual and analysis. The experiment section includes the collection of the flight data or sets the desired acceleration. Moreover, a simplified digital twin that maps the movement of the spindle carts is also implemented in the GUI. The digital twin is to be expanded in the future, so that simulations can be done. With the data gained by the simulations, machine learning techniques could be applied and trained for

monitoring and control purposes. All properties of the former section are also integrated in the manual section. However, there are some more functions implemented, which allow the conduction of different experiments for test purposes. The analysis part contains the presentation of the encoder and acceleration data. Before the system is used, a reference run has to be performed once with the "start init"-bottom of the GUI to determine the zero position of the spindle carts using limit switches. After this, the GUI sets the setup ready for the conduction of the desired experiments.



FIG. 5. GUI of the experiment

## IV. RESULTS

This section presents various results regarding the acceleration of the system based on the accelerometer and the encoder data. Firstly, the results under normal Earth gravity for an analysis of the influence of the flywheels compared to conditions without (in Sect. IV A) will be presented. After that, the results of experiments follow, which have been conducted under Earth's gravity and in microgravity inside the EE (in Sect. IV B). For these test campaigns, the experimental setup of AKUS consisted of the main components including the vacuum chamber, the spindle axes, the motors, and the acceleration sensor. Inside the vacuum chamber was no vacuum, which is only needed for tests with the comet-like samples. Therefore, no samples were used in these tests. Moreover, cables were not routed as planned in the final design, although these are sources of vibrations which may affect the quality of the adjusted accelerations. In addition, during tests inside the EE, the gondola was not evacuated, so that the experiment carrier flew in a normal pressure environment. Since the vacuum in the gondola is mainly used for acoustic decoupling, the normal pressure environment could induce vibrations from any components of the EE inside the experiment.

### A. Influence of the flywheels

As the flywheels play an important role in the control of the motors, this was examined more specifically. Especially, the

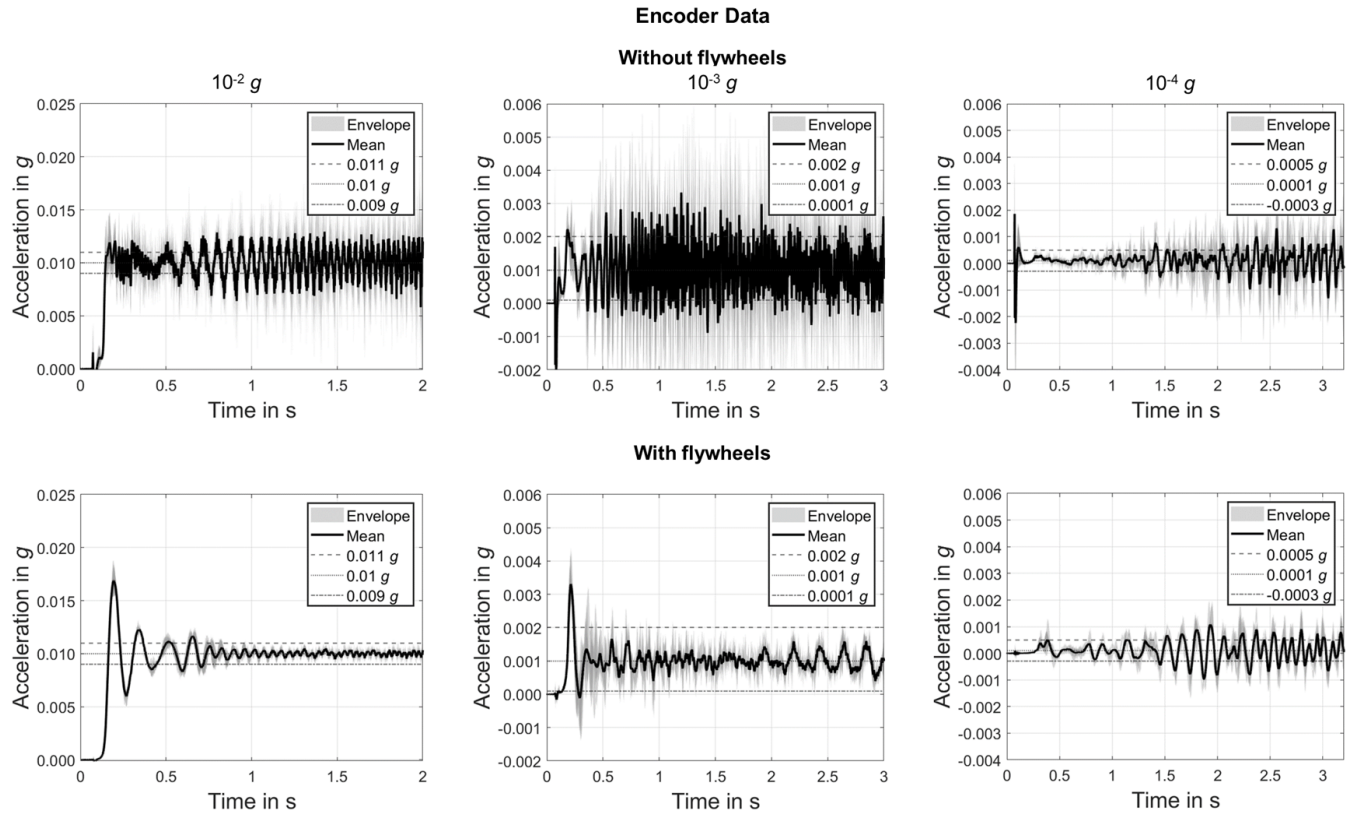


FIG. 6. The encoder data show a positive effect of the flywheels, so that the desired accelerations can be controlled.

acceleration levels  $10^{-2}$ ,  $10^{-3}$  and  $10^{-4} g$  have been investigated with respect to the changes of the motion behavior. For each of these acceleration levels, five experiments have been conducted. In FIG. 6, the envelopes together with the combined mean of the encoder data of the two motors are shown. Those are divided in with and without flywheels based on the adjusted acceleration levels from  $1 \cdot 10^{-2}$  to  $10^{-4}$  (from left to right). The acceleration was recorded over the time. It can clearly be seen that the high frequentative motion and the accelerations' amplitudes of the motors have been smoothed by the flywheels. The flywheels act as low-pass filters for the motors. Although the setup was adjusted for accelerations of  $10^{-2} g$ , as previously described, the motors are capable to simulate gravity levels down to  $10^{-3} g$ . Furthermore, the amplitudes of the frequencies became smaller, leading to a further positive effect generated by the flywheels. However, it is also seen that the controller is not perfectly adjusted, causing large overshoots. As a consequence, the controller needs 0.6 s at the beginning to approach its optimum. In connection with this, the influence of the controller decreases as the adjusted gravity level becomes smaller resulting in a better adaptation to smaller accelerations. From the moment the controller reaches its optimum, the deviations based on the hull curve are approximately  $1 \cdot 10^{-3} g$  at  $10^{-2} g$  regarding the mean plot between 1 and 2 s (in FIG. 6, bottom left). This is also seen at  $10^{-3} g$ . Regarding the combined mean, the

maximum deviation and thus difference from the ideal value is approximately  $\pm 5 \cdot 10^{-4} g$  at  $10^{-3} g$  (FIG. 6, bottom center). With respect to this, the limits of the current system regarding its adjustable acceleration are also shown, which is highlighted in the plots regarding  $10^{-4} g$ , as the amplitudes are too large. In summary, the measurements show the expected improvements by the flywheels. Moreover, they show an improved motor control with maximum deviations of  $\pm 5 \cdot 10^{-4} g$  at  $10^{-3} g$ .

## B. Comparison of Tests under Earth gravity and Microgravity

For the evidence inside the EE, for  $10^{-2}$ ,  $10^{-3}$ , and  $10^{-4} g$  five measurements have been conducted, giving a total of 15 measurements, which are shown in FIG. 7. In these, the mean and the envelopes of five experiments are shown for each gravity level. Besides the encoder data (top), an acceleration sensor has been used additionally to measure the real conditions both with Earth gravity and inside the EE in the microgravity environment (center and bottom). The data from the acceleration sensor has been filtered with a low-pass filter at  $10 \text{ Hz}$ <sup>31</sup>. Furthermore, again the envelope and the combined mean of the encoder data have been added for a better comparison regarding the acceleration data. Comparing the encoder with the acceleration data under Earth gravity, it is seen that those are

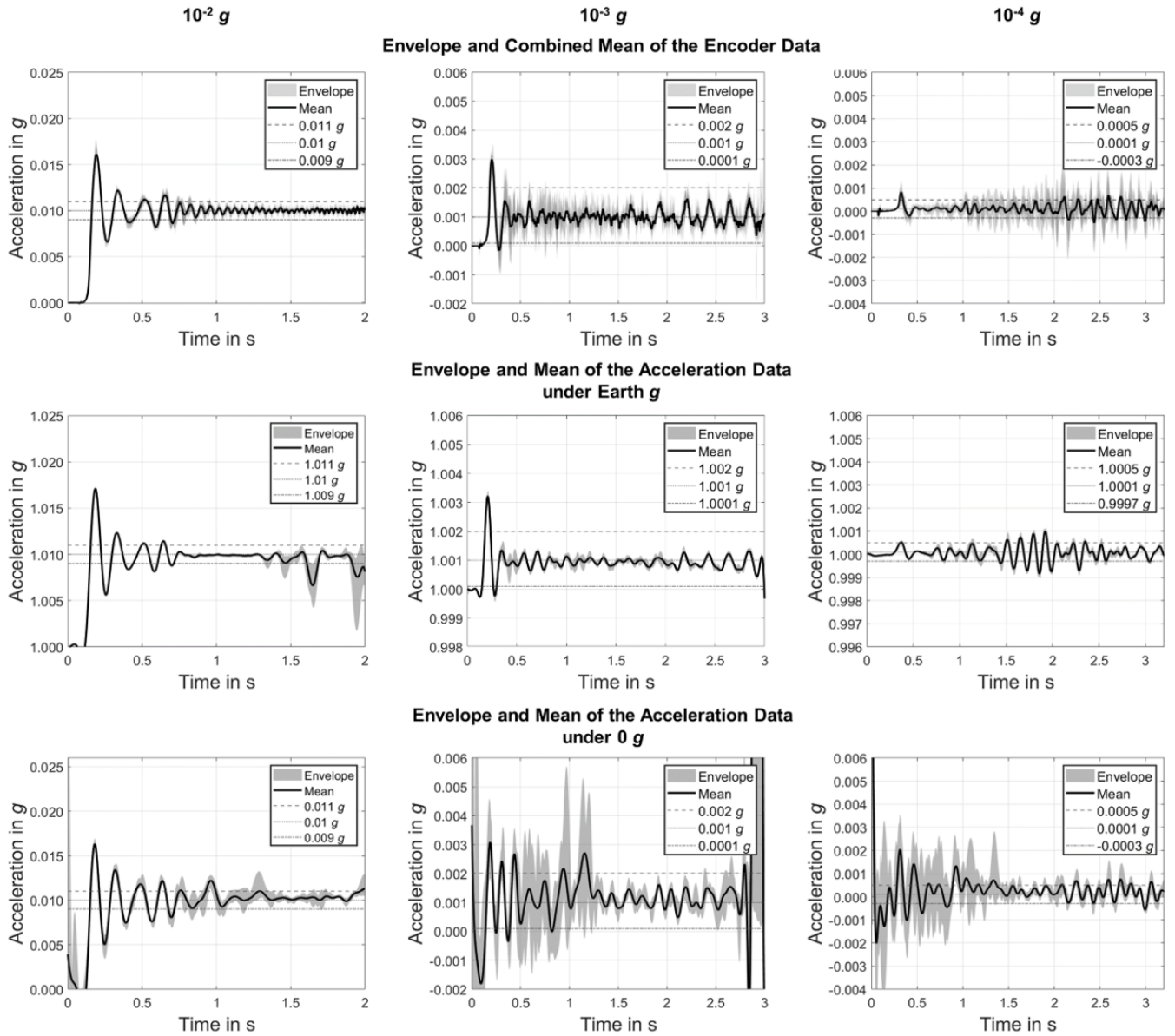


FIG. 7. Comparison regarding the sensors and the environment. The accelerations have been recorded by the encoders (top) and the acceleration sensor (center and bottom). Besides, the data of the acceleration sensor is divided in under Earth  $g$  (center) and microgravity (bottom). The adjusted acceleration are  $10^{-2} g$  (left),  $10^{-3} g$  (center), and  $10^{-4} g$  (right).

similar to each other. Especially, the mean of both encoders and the acceleration data correlate strongly, so that the large oscillations of the secondary motors do not have much influence on the quality of the adjusted acceleration. As described in the previous subsection, the graphs show the typical behavior of the controller at startup, with the amplitudes becoming smaller as the set acceleration decreases. Furthermore, a good acceleration quality of  $10^{-3} g$  is achieved. Another interesting aspect connected to this is that from  $10^{-2}$  to  $10^{-3} g$  under Earth gravity, the acceleration only differs slightly from the adjusted acceleration similar to the encoder data. However, as previously described and expected, a stable acceleration of  $10^{-4} g$  is not detectable with the acceleration sensor, ei-

ther. Nevertheless, the time range from 0.6 s to 1.5 s shows that a stable control of this gravity level should be possible. Moreover, the acceleration graph of  $10^{-2} g$  shows two drops at approximately 1.5 s (FIG. 7 center left). This could be an indicator of a suboptimal motion transmission at higher rotational speeds. The envelope even shows a bigger difference. It is conceivable that the couplings used do not generate enough pressure, so that the centrifugal forces become too great at higher rotational speeds. However, this is not seen in the experiments conducted in the EE as the resistance force is smaller due to the absence of Earth's gravity. In this context, another crucial aspect is indirectly highlighted, which is the necessity of the acceleration sensor. Without it, any kind of

motion transfer errors could not be detected and no clear statements could be made about the acceleration at the examined location since the encoders still show good values regarding their rotational speed. Especially at small accelerations, such as in the range of  $10^{-4} g$ , the formerly mentioned point is a key factor. This is also seen in the bottom graphs in FIG. 7 demonstrating the behavior of the experiments inside the EE. In these, several sources of interference can be seen compared to the graph above regarding Earth's gravity at 0 to 1.4 s. The reason can be an excitation leading to vibrations and therefore residual accelerations caused by the 5 g acceleration phase of the EE. Additionally, as the experiments were conducted under normal atmospheric pressure and not vacuum inside the gondola, also an acoustic excitation of the carrier is possible. As initially mentioned, another source of interference can be the imperfect realization of the experimental setup. This includes cables and other components, which can cause residual vibrations and, consequently, accelerations. In this context, these residual accelerations have to be observed and considered during the conduction of the experiments. Besides all of this and after the excitation phase, the quality of the adjusted acceleration approaches the same level as under Earth's gravity at  $10^{-3}$  and  $10^{-4} g$ . As a result, those interference sources do not have a major influence at higher accelerations, such as in the  $10^{-2} g$  regime. Consequently, the system shows a good performance at higher gravity levels. In summary, the results demonstrate on the one hand that an acceleration-based control is necessary to achieve constant accelerations in contrast to an encoder-based control. On the other hand, the results can be considered positive, giving potential for improvements and therefore better results in the future.

## V. DISCUSSION

The results indicate that the developed acceleration system of AKUS, based mainly on two servo motors and the spindle axes, is in general able to generate the desired accelerations. However, the added flywheels are required for this. As presented before, most of the servo motors are not designed to generate small constant acceleration torques, which is also shown in FIG. 4. Using the flywheels, the inertia of the whole system becomes higher, resulting in a sufficient motion behavior and therefore constant accelerations, which is presented in FIG. 7. In addition, the motor encoders show a good performance down to an acceleration of  $10^{-3} g$ . The maximum deviation here is approximately at  $5 \cdot 10^{-4} g$ , although the flywheels were designed for the higher limit, namely  $10^{-2} g$ . In this context, an adjustment of the system using flywheels with higher inertia can contribute to a better performance in the area of  $10^{-4} g$ . Furthermore, the described results have also been reflected by the acceleration sensor under Earth's gravity conditions. Moreover, the mean of the accelerations generated by both motors appeared to be similar to the ones recorded by the acceleration sensor, so that the large amplitudes of the secondary motor, which are generated to adjust to the primary motor, have no negative effects. Nevertheless, for higher accelerations starting at  $10^{-3} g$ , the controller shows

significant transient responds with a high first overshoot, indicating that the control parameters have to be adjusted for these accelerations. Improving these parameters will lead to a quicker and an improved steady state condition of the system with smaller deviations. Nevertheless, this behavior is negligibly small at  $10^{-4} g$  since the amplitudes occurring at this acceleration level are nearly the same. At accelerations of  $10^{-2} g$  tested under Earth gravity and lower accelerations tested under microgravity, the importance of the acceleration sensor is highlighted due to its ability to record accelerations at the examined localization. Due to this fact, it is also able to detect movement errors or interference sources in the environment. Furthermore, a dynamic control of the acceleration is necessary as the experiments conducted in microgravity indicate. This was also intended from the beginning and is planned in the future.

## VI. CONCLUSION AND OUTLOOK

Currently, SSSB research primarily depends on time and plan-consuming space missions. Although such missions are important for the validation of diverse theories, there have been only few of them. Consequently, it is important to develop Earth-bounded alternatives, which enable the research of these objects in realistic environments. Besides vacuum and low temperature conditions, a key aspect is the enabling of gravity levels between  $10^{-2}$  and  $10^{-4} g$ , which are present on these objects. For this reason, an acceleration system has been developed within the AKUS project to enable such conditions inside the EE, a third generation drop tower. The acceleration system is based on two drive trains each consisting of a servo motor and a spindle axis. The system will move a SSSB-simulant on an accelerated trajectory within a vacuum chamber. However, servo motors are not designed to enable such small accelerations as the main purpose of those motors is to perform position- and speed-based tasks. Therefore, adjusted motors with longer shafts and implemented flywheels designed to enable accelerations around  $10^{-2} g$  have been added to the motor shafts to increase the system inertia. General tests showed that the flywheels improve the motion behavior as expected. In addition to the encoder-based data, an acceleration sensor placed on the sample holder was used to verify the results besides the encoders. These data confirmed that the motors are capable to simulate the desired acceleration with the adjustments described. The system even achieved acceleration conditions with maximum deviations of approximately  $\pm 5 \cdot 10^{-4} g$  at  $10^{-3} g$ , which exceeded our expectations. For this reason, it can be assumed that the motors can deliver better results together with further adjustments, so that the lower limit of  $10^{-4} g$  can be achieved in the future. Nevertheless, some mechanical adjustments, such as new couplings or larger flywheels for the smaller accelerations, have to be made to improve the whole system.

As a result, an overall improvement of the system is one major goal in the future, so that scientific experiments based on the comet-like samples can be conducted. Furthermore, more tests have to be conducted especially to provide sta-

ble accelerations in the full range. In this context, the controller has to be optimized as the current results showed significant overshoots starting at accelerations of  $10^{-3} g$  and higher. Moreover, alternative control concepts have to be developed, such as a cascade control based on sensor fusion using the encoders and the acceleration sensor. Especially the implementation of the acceleration sensor for control is an important step to improve the system. This has to be considered with respect to the residual acceleration of the EE at the beginning of the microgravity time. In addition, tests have to be done with flywheels designed for the smaller accelerations as the addition of the former flywheels in general improved the system enabling most of the accelerations, which are necessary to conduct the desired experiments. In this context, firstly tests in vacuum and finally test with the comet-like sample will be performed in the near future as this is the main goal of the project AKUS. As a result, the entire system has to be built up including the cameras, which are necessary to observe the sample depending on the acceleration. The setup can be used for the study of SSSB such as comets and asteroids, providing an Earth-bounded alternative to space missions and leading to international research projects.

## ACKNOWLEDGMENTS

The authors would like to thank the German Space Agency within the German Aerospace Center (DLR) and the Federal Ministry for Economic Affairs and Climate Action (BMWK) on the basis of a decision by the German Bundestag (FKZ: 50WM2254). Moreover, we would like to thank the DFG and the Lower Saxony state government for their financial support for building the Hannover Institute of Technology (HITec) and the Einstein-Elevator (NI1450004, INST 187/624-1 FUGB) as well as the Institute for Satellite Geodesy and Inertial Sensing of the German Aerospace Center (DLR-SI) for the development and the provision of the experiment carrier system. Further funding was provided by the D-A-CH program (DFG: GU 1620/3-1 and BL 298/26-1, project number 395699456; SNF: 200021E 177964; FWF: I 3730-N36) of the CoPhyLab, the European Union under grant agreement NO. 101081937 – Horizon 2022 - Space Science and Exploration Technologies (views and opinions expressed are however those of the authors only and do not necessarily reflect those of the European Union; neither the European Union nor the granting authority can be held responsible for them) and the Niedersächsisches Vorab in the framework of the research cooperation between Israel and Lower Saxony under grant ZN 3630.

We would also like to thank Jan Hoffmann and Mohammad Ibrahim for their contributions during their student work.

## AUTHOR DECLARATIONS

### Conflict of Interest

The authors declare no conflicts of interest.

## Special Unit

$$g = \text{Earth's gravity } (1 g = 9.81 \text{ m/s}^2)$$

## DATA AVAILABILITY STATEMENT

The datasets used and/or analysed during the current study are available from the corresponding author or the co-authors on reasonable request.

<sup>1</sup>A. F. Cheng, H. F. Agrusa, B. W. Barbee, A. J. Meyer, T. L. Farnham, S. D. Raducan, D. C. Richardson, E. Dotto, A. Zinzi, V. Della Corte, T. S. Statler, S. Chesley, S. P. Naidu, M. Hirabayashi, J.-Y. Li, S. Eggel, O. S. Barnouin, N. L. Chabot, S. Chocron, G. S. Collins, R. T. Daly, T. M. Davison, M. E. DeCoster, C. M. Ernst, F. Ferrari, D. M. Graninger, S. A. Jacobson, M. Jutzi, K. M. Kumamoto, R. Luther, J. R. Lyzhoft, P. Michel, N. Murdoch, R. Nakano, E. Palmer, A. S. Rivkin, D. J. Scheeres, A. M. Stickle, J. M. Sunshine, J. M. Trigo-Rodríguez, J.-B. Vincent, J. D. Walker, K. Wünnemann, Y. Zhang, M. Amoroso, I. Bertini, J. R. Brucato, A. Cappanolo, G. Cremonese, M. Dall'Ora, P. J. D. Deshpriya, I. Gai, P. H. Haselmann, S. Ieva, G. Impresario, S. L. Ivanovski, M. Lavagna, A. Lucchetti, E. M. Epifani, D. Modenini, M. Pajola, P. Palumbo, D. Perna, S. Pirrotta, G. Poggiali, A. Rossi, P. Tortora, M. Zannoni, and G. Zanotti, "Momentum transfer from the dart mission kinetic impact on asteroid dimorphos," *Nature* **616**, 457–460 (2023).

<sup>2</sup>D. S. Lauretta, S. S. Balram-Knutson, E. Beshore, W. V. Boynton, C. Drouet d'Aubigny, D. N. DellaGiustina, H. L. Enos, D. R. Golish, C. W. Hergenrother, E. S. Howell, C. A. Bennett, E. T. Morton, M. C. Nolan, B. Rizk, H. L. Roper, A. E. Bartels, B. J. Bos, J. P. Dworkin, D. E. Highsmith, D. A. Lorenz, L. F. Lim, R. Mink, M. C. Moreau, J. A. Nuth, D. C. Reuter, A. A. Simon, E. B. Bierhaus, B. H. Bryan, R. Ballouz, O. S. Barnouin, R. P. Binzel, W. F. Botke, V. E. Hamilton, K. J. Walsh, S. R. Chesley, P. R. Christensen, B. E. Clark, H. C. Connolly, M. K. Crombie, M. G. Daly, J. P. Emery, T. J. McCoy, J. W. McMahon, D. J. Scheeres, S. Messenger, K. Nakamura-Messenger, K. Righter, and S. A. Sandford, "Osiris-rex: Sample return from asteroid (101955) bennu," *Space Science Reviews* **212**, 925–984 (2017).

<sup>3</sup>R. E. March, "Osiris-rex: a nasa asteroid space mission," *International Journal of Mass Spectrometry* **469**, 116677 (2021).

<sup>4</sup>R. T. Daly, C. M. Ernst, O. S. Barnouin, N. L. Chabot, A. S. Rivkin, A. F. Cheng, E. Y. Adams, H. F. Agrusa, E. D. Abel, A. L. Alford, E. I. Asphaug, J. A. Atchison, A. R. Badger, P. Baki, R.-L. Ballouz, D. L. Bekker, J. Bellerose, S. Bhaskaran, B. J. Buratti, S. Cambioni, M. H. Chen, S. R. Chesley, G. Chiu, G. S. Collins, M. W. Cox, M. E. DeCoster, P. S. Ericksen, R. C. Espiritu, A. S. Faber, T. L. Farnham, F. Ferrari, Z. J. Fletcher, R. W. Gaskell, D. M. Graninger, M. A. Haque, P. A. Harrington-Duff, S. Hefter, I. Herreros, M. Hirabayashi, P. M. Huang, S.-Y. W. Hsieh, S. A. Jacobson, S. N. Jenkins, M. A. Jensenius, J. W. John, M. Jutzi, T. Kohout, T. O. Krueger, F. E. Laipert, N. R. Lopez, R. Luther, A. Lucchetti, D. M. Mages, S. Marchi, A. C. Martin, M. E. McQuaide, P. Michel, N. A. Moskovitz, I. W. Murphy, N. Murdoch, S. P. Naidu, H. Nair, M. C. Nolan, J. Ormö, M. Pajola, E. E. Palmer, J. M. Peachey, P. Pravec, S. D. Raducan, K. T. Ramesh, J. R. Ramirez, E. L. Reynolds, J. E. Richman, C. Q. Robin, L. M. Rodriguez, L. M. Roufberg, B. P. Rush, C. A. Sawyer, D. J. Scheeres, P. Scheirich, S. R. Schwartz, M. P. Shannon, B. N. Shapiro, C. E. Shearer, E. J. Smith, R. J. Steele, J. K. Steckloff, A. M. Stickle, J. M. Sunshine, E. A. Superfin, Z. B. Tarzi, C. A. Thomas, J. R. Thomas, J. M. Trigo-Rodríguez, B. T. Tropic, A. T. Vaughan, D. Velez, C. D. Waller, D. S. Wilson, K. A. Wortman, and Y. Zhang, "Successful kinetic impact into an asteroid for planetary defence," *Nature* **616**, 443–447 (2023).

<sup>5</sup>C. Kreuzig, G. Kargl, A. Pommerol, J. Knollenberg, A. Lethuillier, N. S. Molinski, T. Gilke, D. Bischoff, C. Feller, E. Kührt, H. Sierks, N. Hänni, H. Capelo, C. Güttler, D. Haack, K. Otto, E. Kaufmann, M. Schweighart, W. Macher, P. Tiefenbacher, B. Gundlach, and J. Blum, "The cophylab comet-simulation chamber," *Review of Scientific Instruments* **92**, 115102 (2021).

- <sup>6</sup>D. W. G. SEARS, H. W. KOCHAN, and W. F. HUEBNER, “Laboratory simulation of the physical processes occurring on and near the surfaces of comet nuclei,” *Meteoritics & Planetary Science* **34**, 497–525 (1999).
- <sup>7</sup>K. J. Seidensticker, H. Kochan, and D. Möhlmann, “The dlr small simulation chamber: A tool for cometary research in the lab,” *Advances in Space Research* **15**, 29–34 (1995).
- <sup>8</sup>C. Lotz, T. Froböse, A. Wanner, L. Overmeyer, and W. Ertmer, “Einstein-elevator: A new facility for research from  $\mu\text{g}$  to 5 g,” *Gravitational and Space Research* **5**, 11–27 (2017).
- <sup>9</sup>C. Zhang, C. Yang, L. Hu, S. Chen, Y. Zhao, L. Duan, and Q. Kang, “Beijing drop tower microgravity adjustment towards 10<sup>-3</sup> ~ 10<sup>-5</sup>g level by cold-gas thrusters,” *Microgravity Science and Technology* **35**, 1–18 (2023).
- <sup>10</sup>C. Lotz, *Untersuchungen zu Einflussfaktoren auf die Qualität von Experimenten unter Mikrogravitation im Einstein-Elevator* (Hannover : Institutionelles Repositorium der Leibniz Universität Hannover, 2022).
- <sup>11</sup>G. H. Schwehm and R. Schulz, “The international rosetta mission,” in *Laboratory Astrophysics and Space Research*, Astrophysics and Space Science Library, edited by P. Ehrenfreund, C. Krafft, H. Kochan, and V. Pirronello (Springer, Dordrecht, 1999) pp. 537–546.
- <sup>12</sup>D. S. Lauretta, H. C. Connolly, J. E. Aebersold, C. M. O. Alexander, R.-L. Ballouz, J. J. Barnes, H. C. Bates, C. A. Bennett, L. Blanche, E. H. Blumenfeld, S. J. Clemett, G. D. Cody, D. N. DellaGiustina, J. P. Dworkin, S. A. Eckley, D. I. Foustoukos, I. A. Franchi, D. P. Glavin, R. C. Greenwood, P. Haenecour, V. E. Hamilton, D. H. Hill, T. Hiroi, K. Ishimaru, F. Jourdan, H. H. Kaplan, L. P. Keller, A. J. King, P. Koefoed, M. K. Kontogiannis, L. Le, R. J. Macke, T. J. McCoy, R. E. Milliken, J. Najorka, A. N. Nguyen, M. Pajola, A. T. Polit, K. Righter, H. L. Roper, S. S. Russell, A. J. Ryan, S. A. Sandford, P. F. Schofield, C. D. Schultz, L. B. Seifert, S. Tachibana, K. L. Thomas-Keprta, M. S. Thompson, V. Tu, F. Tusberty, K. Wang, T. J. Zega, and C. W. V. Wolner, “Asteroid (101955) bennu in the laboratory: Properties of the sample collected by osiris – rex,” *Meteoritics & Planetary Science* **59**, 2453–2486 (2024).
- <sup>13</sup>A. V. Ivanova, “Small bodies of the solar system active at large heliocentric distances: Studies with the 6-meter telescope of sao ras,” *Astrophysical Bulletin* **75**, 31–49 (2020).
- <sup>14</sup>S. C. Lowry and A. Fitzsimmons, “William herschel telescope observations of distant comets,” *Monthly Notices of the Royal Astronomical Society* **358**, 641–650 (2005).
- <sup>15</sup>C. Kreuzig, J. N. Brecher, G. Meier, C. Schuckart, N. S. Molinski, J. Pfeifer, J. Markkanen, C. Knoop, M. Timpe, M. Goldmann, J. Knollenberg, B. Gundlach, and J. Blum, “Illuminated granular water ice shows ‘dust’ emission,” *Astronomy & Astrophysics* **693**, A258 (2025).
- <sup>16</sup>D. Bockelée-Morvan and N. Biver, “The composition of cometary ices,” *Philosophical transactions. Series A, Mathematical, physical, and engineering sciences* **375** (2017), 10.1098/rsta.2016.0252.
- <sup>17</sup>C. Kreuzig, D. Bischoff, N. S. Molinski, J. N. Brecher, A. Kovalev, G. Meier, J. Oesert, S. N. Gorb, B. Gundlach, and J. Blum, “Micrometre-sized ice particles for planetary science experiments – cophylab cryogenic granular sample production and storage,” *RAS Techniques and Instruments* **2**, 686–694 (2023).
- <sup>18</sup>T. Y. Liu, Q. P. Wu, B. Q. Sun, and F. T. Han, “Microgravity level measurement of the beijing drop tower using a sensitive accelerometer,” *Scientific Reports* **6**, 31632 (2016).
- <sup>19</sup>S. H. Wan, M. G. Yin, X. D. Guan, H. Lin, J. C. Xie, and W.-R. Hu, “Drop tower beijing and short-time microgravity experiments,” *38th COSPAR Scientific Assembly* **38**, 2 (2010).
- <sup>20</sup>K. Joeris, M. Keulen, and J. E. Kollmer, “Controlled partial gravity platform for milligravity in drop tower experiments,” *Review of Scientific Instruments* **96** (2025), 10.1063/5.0233405.
- <sup>21</sup>P. von Kampen, U. Kaczmarczik, and H. J. Rath, “The new drop tower catapult system,” *Acta Astronautica* **59**, 278–283 (2006).
- <sup>22</sup>T. Könemann, A. Gierse, P. von Kampen, and M. Avila, “The gravitower bremen pro - experiences with a next-generation drop tower system,” *44th COSPAR Scientific Assembly, Held 16-24 July* **44**, 2951 (2022).
- <sup>23</sup>O. Anton, I. Bröckel, D. Derr, A. Fieguth, M. Franzke, M. Gärtner, E. Giese, J. S. Haase, J. Hamann, A. Heidt, S. Kanthak, C. Klempt, J. Kruse, M. Krutzik, S. Kubitzka, C. Lotz, K. Müller, J. Pahl, E. M. Rasel, M. Schiemangk, W. P. Schleich, S. Schwertfeger, A. Wicht, and L. Wörner, “Intentas - an entanglement-enhanced atomic sensor for microgravity,” *EPJ Quantum Technology* **12** (2025), 10.1140/epjqt/s40507-025-00330-9.
- <sup>24</sup>C. Garcion, S. S. Gill, M. Misslisch, A. Heidt, I. Papadakis, B. Piest, V. Schkolnik, T. Wendrich, A. Prat, K. Bleeke, H. Müntinga, M. Krutzik, S.-w. Chiow, N. Yu, C. Lotz, N. Gaaloul, and E. M. Rasel, “Dark energy search by atom interferometry in the einstein-elevator,” *EPJ Quantum Technology* **12**, 1–21 (2025).
- <sup>25</sup>J. Raffel, T. Böhm, J. Düsing, M. Röhl, C. Schilde, A. P. Malshe, L. Overmeyer, and C. Lotz, “Ultrasonic levitation as a handling tool for in-space manufacturing processes,” *Journal of Manufacturing Science and Engineering* **146** (2024), 10.1115/1.4066335.
- <sup>26</sup>M. Raupert, M. Pusch, E. Tahtali, R. Sperling, A. Heidt, C. Lotz, A. Katterfeld, and L. Overmeyer, “Laser metal deposition with metal powder in microgravity,”
- <sup>27</sup>R. Sperling, M. Raupert, C. Lotz, and L. Overmeyer, “Simulative validation of a novel experiment carrier for the einstein-elevator,” *Scientific Reports* **13**, 19366 (2023).
- <sup>28</sup>J. Li, J. Su, M. Gao, D. Zhao, L. Zhang, D. Wang, and F. Shi, “Inertia matching of cnc cycloidal gear form grinding machine servo system,” *Mechanics & Industry* **24**, 31 (2023).
- <sup>29</sup>“Beckhoff information system - german,” (22.08.2025).
- <sup>30</sup>“Three essential factors for servo motor sizing | electromate inc,” (22.08.2025).
- <sup>31</sup>K. McPherson, E. Kelly, and J. Keller, “Acceleration environment of the international space station,” in *47th AIAA Aerospace Sciences Meeting including The New Horizons Forum and Aerospace Exposition* (American Institute of Aeronautics and Astronautics, Reston, Virginia, 2009).
- <sup>32</sup>G. Martin, “Newspace: The emerging commercial space industry,”